# 3D Beamforming with Multi-Active Multi-Passive Antenna Arrays Using Stochastic Optimization

Georgios K. Papageorgiou*, Mathini Sellathurai*, Dimitrios K. Ntaikos†, Constantinos B. Papadias‡

*Heriot-Watt University, Edinburgh, UK, Email: {g.papageorgiou, m.sellathurai}@hw.ac.uk

†Athens Information Technology, Athens, GR, Email: dint@ait.gr

‡The American College of Greece, Athens, GR, Email: cpapadias@acg.edu

*Abstract*—In this paper, we consider the 3D beamforming with Multi-Active Multi-Passive (MAMP) antenna arrays. For the optimization of the hybrid array's active elements' (AEs) weights and passive elements' (PEs) loads, we propose a novel algorithm, i.e., the alternating optimization - stochastic 3D beamforming algorithm (AO-S3DBA). The scheme is built on a generalized cost function and alternates between the optimization of the loads and weights. Despite the dramatic increase in data points, we managed to decrease the algorithm's complexity by employing Adam, a popular accelerator for stochastic optimization, for the update of the optimization variables. We present simulation results, where the proposed MAMP array can successfully emulate the beam of a uniform rectangular array (URA) with the use of 50% less AEs and with beam steering capabilities towards various azimuth and elevation directions. We believe that this newly proposed type of hybrid transceiver offers a good trade-off between cost and performance, which can be particularly useful in many industrial and Internet-of-Things (IoT) applications, where the deployment of a large number of transceivers / sensors directly affects the application's total cost.

*Index Terms*—Multi-active multi-passive MAMP arrays, hybrid arrays, 3D beamforming, Adam, alternating optimization stochastic 3D beamforming algorithm

## I. INTRODUCTION

Electronically steerable passive array radiators (ESPARs), which are typically considered having a single-RF (Radio Frequency) chain [1], [2], offer the potential to increase channel capacity, enhance quality-of-service, improve RF spectrum usage and reduce power consumption of wireless networks [3]. Moreover, they can be particularly beneficial for industrial and IoT applications, where low cost and power consumption is often the driving force for various applications. Multi-Active Multi-Passive (MAMP) antenna arrays, which are the evolution of ESPARs, are considered hybrid designs composed of multiple AEs and PEs. The AEs of the MAMP arrays admit both phase and amplitude adjustments (weights), whereas the PEs (passive in the sense that they are not connected to an active RF chain) are controlled by variable loads [4] via the adjustment typically of the imaginary part only (real part should ideally be zero to avoid losses). Hence, the far field radiation pattern is modified accordingly. Other popular hybrid designs consist of AEs and phase shifters [5], [6]. In contrast to ESPARs, MAMP arrays have demonstrated better capabilities in beamforming [7], as compared to their single AE counterparts [8], [9], [10]. Transition from single element ESPARs to MAMP arrays is far from trivial, due to: a) the hybrid nature that complicates the design (optimal half-wavelength spacing between AEs and closer spacing between the PEs is required for enhanced mutual coupling) and b) the necessity to jointly optimize the PE variable loads and the AE weights. The latter is a combinatorial task for discrete values of loads. In the related literature with single AE ESPARs, the common practice was to optimize their values exhaustively (for a small number of PEs) [1], [3], [11], [12]. However, this approach is prohibitive for large numbers of PEs, as is the case especially for massive MAMP arrays.

A joint load-weight optimization was recently introduced in [7], where we proposed a novel algorithm based on alternating optimization for the values of the PE loads and the AE weights. It was demonstrated there that the azimuth plane radiation pattern of a uniform linear array (ULA) can be emulated by a MAMP array with a reduced number of AEs. However, in practice, both the azimuth and elevation angles should exhibit good properties (e.g., steering capability, reduced side-lobes, etc.). This is the research direction of this work, since this is not guaranteed by optimizing the azimuth pattern only as in [7].

In this paper, we address the 3-dimensional (3D) beamforming of MAMP arrays in an attempt to emulate the beam of a URA. To this end, we propose a novel algorithm for the joint optimization of the load and weight values using a stochastic optimization approach over a generalized cost function. Furthermore, we employed a popular accelerator for stochastic optimization known as Adam [13], in order to reduce the computational complexity of the method in the random search steps. To the best of our knowledge, this is the first time that optimization for 3D beamforming has been studied in the literature related to MAMP arrays or ESPARs.

## II. 3D BEAMFORMING WITH MAMP ARRAYS

In this section, we present the 3D modeling of the MAMP arrays. The normalized steering vector of an antenna array with $N$ elements (active, passive or both), regardless of its selected layout (geometry), at azimuth angle $\phi \in \mathcal{G} = [0, 2\pi)$ and elevation angle $\theta \in \mathcal{F} = [0, \pi]$ can be expressed as:

$$\mathbf{a}(\phi, \theta) = \left[ e^{\mathrm{i}\,\kappa \mathbf{r}_1^T \mathbf{u}(\phi,\theta)}, \ldots, e^{\mathrm{i}\,\kappa \mathbf{r}_N^T \mathbf{u}(\phi,\theta)} \right]^T / \sqrt{N}, \qquad (1)$$

where $\kappa = 2\pi/\lambda$, $\lambda = c/f$ is the wavelength of the frequency $f$ ($c$ is the speed of light), $\mathbf{u}(\phi, \theta) = [\sin\theta\cos\phi, \sin\theta\sin\phi, \cos\theta]^T$ is the point on the unit sphere in $\mathbb{R}^3$ and $\mathbf{r}_n \in \mathbb{R}^3$ are the coordinates of the $n$-th antenna array element for $n = 1, \ldots, N$. It should be noted that the advantage of using the notation in (1) is its generality, since it can be used with arbitrary array layout, i.e., rectangular, circular, etc. The (normalized) beam pattern of the array is given by the amplitude of the complex matrix with elements:

$$\left(\mathbf{B}(\phi, \theta)\right)_{i,j} = \mathbf{a}(\phi, \theta)^H \mathbf{a}(\phi_i, \theta_j), \qquad (2)$$

for every $j \in \mathcal{S}_\mathcal{G} \subset \mathcal{G}, i \in \mathcal{S}_\mathcal{F} \subset \mathcal{F}$, where the sets $\mathcal{S}_\mathcal{G}$ and $\mathcal{S}_\mathcal{F}$ correspond to countable subsets of $\mathcal{G}$ and $\mathcal{F}$ (grids), respectively.

In our design, we consider a rectangular MAMP array (R-MAMP) consisting of $N_a$ AEs (dipoles) whose centers lie in the $x$-axis (parallel to the $z$-axis) equally spaced at $\lambda/2$, and, $N_p$ (even number for symmetry) PEs per active. The PEs are positioned along the $y$-axis and spaced at a distance of $p\lambda$ from each other (where $p < 0.5$ to enhance the mutual coupling). The dipoles are considered linear and ideal (no losses) of length $l = \lambda/2$ and radius $r = \lambda/100$. The total number of elements is denoted as $N = N_a(N_p + 1)$. An R-MAMP array design with 4 AEs and 24 PEs (4A-24P) can be found in [7]. Let $\mathbf{Z}$ denote the impedance matrix (taking into account all coupling), which (for ideal dipoles) is calculated analytically [14]. The set of indices $\mathcal{A} = \{1, \ldots, N\}$ of all elements is separated into two disjoint subsets, i.e., $\mathcal{S}$ and $\mathcal{S}^c = \mathcal{A} \setminus \mathcal{S}$, corresponding to the AEs and PEs, respectively.

The beam pattern of a MAMP array is calculated from (2) by replacing $\mathbf{a}(\phi, \theta)$ with the conjugate of the current vector. The current vector of a MAMP array is given by

$$\mathbf{i} = \mathbf{i}(\mathbf{x}, \mathbf{v}) = \left(\mathbf{Z} + \text{diag}(\mathbf{x})\right)^{-1} \mathbf{v},$$

where $\mathbf{v}$ is the voltage vector with non-zero complex values corresponding to its AEs (thus $\mathbf{v}_{\mathcal{S}^c} = \mathbf{0}$) and $\text{diag}(\mathbf{x})$ is the diagonal matrix with the values of the vector $\mathbf{x}$ on its main diagonal. Moreover,

$$\mathbf{x} = \mathbf{I}_\mathcal{S} \mathbf{x}_\mathcal{S} + \mathbf{I}_{\mathcal{S}^c} \mathbf{x}_{\mathcal{S}^c} = \left[\mathbf{x}_1^T, \ldots, \mathbf{x}_{N_a}^T\right]^T \qquad (3)$$

is the load reactance vector that controls the radiation pattern of the MAMP array (vector $\mathbf{x}$ decomposed into two disjoint parts), where $\mathbf{I}$ is the identity matrix and $\mathbf{I}_\mathcal{S}$ denotes its columns restricted over the set $\mathcal{S}$. Each vector $\mathbf{x}_j$ (at the right-hand side of Eq. (3)), $j = 1, \ldots, N_a$, corresponds to the loads of the $j$-th cluster of elements of the MAMP array with values

$$\mathbf{x}_j = \left[\text{i}\,\mathbf{x}_j^t, R_a, \text{i}\,\mathbf{x}_j^b\right]^T, \qquad (4)$$

where $R_a \in \mathbb{R}_+$ is the input impedance of each AE, $\text{i}^2 = -1$, while the rest of its entries, i.e., $\mathbf{x}_j^t = [x_j(1), \ldots, x_j(N_p/2)]$ and $\mathbf{x}_j^b = [x_j(N_p/2 + 1), \ldots, x_j(N_p)]$ correspond to the PE load values (in increasing order of the $y$-axis). The antenna gain of the MAMP array is given by:

$$\mathbf{G}(\phi, \theta) = \eta \mathbf{D}(\phi, \theta), \qquad (5)$$

where $\eta \in [0, 1]$ is the antenna efficiency (for $\eta = 1$ no losses are assumed),

$$\mathbf{D}(\phi, \theta) = \frac{\int_0^{2\pi} \int_0^\pi S(\phi, \theta) |\mathbf{B}(\phi, \theta)|^2 \sin\theta \, d\theta \, d\phi}{(1/4\pi) \int_0^{2\pi} \int_0^\pi |\mathbf{B}(\phi, \theta)|^2 \sin\theta \, d\theta \, d\phi} \qquad (6)$$

is the antenna distributed directivity and $S(\phi, \theta)$ is the normalized radiation intensity defined as the power per unit solid angle [15]. From (5), (6) it is evident that the gain is directly affected by the beam pattern of the array. Our goal is to reproduce the beam pattern of an all-active array using an R-MAMP with as few AEs as possible.

## III. AN ALTERNATING OPTIMIZATION - STOCHASTIC 3D BEAMFORMING ALGORITHM FOR MAMP ARRAYS

In this section we introduce an algorithm for emulating the 3D beam pattern of a URA using the R-MAMP of Section II. Therefore: a) we extend the use of the algorithm presented in [7] to the 3D beamforming case by using a generalization of the cost function and b) we accelerate the convergence of the method by using Adam.

The generalization of the 2D model to the 3D beamforming is achieved by using the matrix inner product, i.e, the trace operator denoted as $\text{tr}(\cdot)$. Thus, we employ the *cross correlation coefficient* (CCC), which represents a similarity measure between the radiated 3D beams and is a function of both the loads and the voltage vector. For a selected MAMP array layout, which is determined by the set $\mathcal{S}$ of AEs and the set $\mathcal{S}^c$ of PEs with corresponding impedance matrix $\mathbf{Z}$, the cost function that we attempt to minimize (equivalent to CCC maximization) is expressed as:

$$L(\mathbf{x}_{\mathcal{S}^c}, \mathbf{w}) = 1 - \frac{\left|\text{tr}\left(\mathbf{B}^H \mathbf{A}(\mathbf{x}_{\mathcal{S}^c}, \mathbf{w})\right)\right|}{\|\mathbf{B}\|_F \|\mathbf{A}(\mathbf{x}_{\mathcal{S}^c}, \mathbf{w})\|_F}, \qquad (7)$$

where $\mathbf{B} = \mathbf{B}(\theta, \phi)$ is the desired complex matrix (corresponding to the beam pattern) of a full active antenna array whose beam we wish to emulate, $\|\cdot\|_F$ denotes the Frobenius norm of a matrix and

$$\left(\mathbf{A}(\mathbf{x}_{\mathcal{S}^c}, \mathbf{w})\right)_{i,j} = \mathbf{v}^T(\mathbf{w})\left(\mathbf{Z} + \text{diag}(\mathbf{x})\right)^{-1} \mathbf{a}_M(\phi_i, \theta_j). \qquad (8)$$

The steering vector of the MAMP array with elements in $\mathcal{A} = \mathcal{S} \cup \mathcal{S}^c$ is denoted as $\mathbf{a}_M(\phi_i, \theta_j)$ and is given by (1); $\mathbf{v}(\mathbf{w}) = \mathbf{I}_\mathcal{S}\left(\mathbf{w}_{1:N_a} + \text{i}\,\mathbf{w}_{(N_a+1):2N_a}\right)$ is the voltage vector, where $\mathbf{w} = \left[\mathfrak{R}(\mathbf{v}_\mathcal{S}^T), \; \mathfrak{I}(\mathbf{v}_\mathcal{S}^T)\right]^T$ and $\mathbf{x}$ is given by (3).

The minimization of (7) with respect to both variables $\mathbf{x}_{\mathcal{S}^c}$ and $\mathbf{w}$ is non-convex (considering values in the continous domain). Therefore, standard optimization techniques do not apply here. Next, we highlight the major differences between the 2D model in [7] and the proposed 3D beamforming model. First of all, we generalize the cost function to the one in (7). However, the transition to 3D beam patterns results in an increase of the total complexity of the method, since both $\mathbf{A}$ and $\mathbf{B}$ are now large dimensional matrices (e.g., $1°$ resolution in both azimuth and elevation leads to more than 65K entries per matrix). Therefore, the slow convergence of stochastic gradient descent (SGD) does not scale well with

the problem. To this end, we employed the Adam [13], which is an algorithm for first-order gradient-based optimization of stochastic objective functions, based on adaptive estimates of lower-order moments (also used for the training of deep neural networks). As a result, we managed to decrease the running time from several hours to approximately 15 minutes using MATLAB R2018b on a PC running Windows 10 with Intel i7-6700 CPU at 3.40GHz. The proposed iterative algorithm for the 3D beamforming of MAMP arrays, i.e., AO-S3DBA in Alg. 1, is based on alternating optimization between its two parameters, $\mathbf{x}_{\mathcal{S}^c}$ and $\mathbf{w}$.

---

**Algorithm 1** Alternating Optimization - Stochastic 3D Beamforming Algorithm (AO-S3DBA)

---

1: **procedure** AO-S3DBA($\mathbf{B}, \mathcal{S}, \mathbf{Z}, \boldsymbol{\beta}, \tau, N_m, T_{er}, \epsilon, b_1, b_2$)
2:    $m \leftarrow 0$, $\mathbf{x}_{\mathcal{S}^c} = \mathbf{0}$, $\mathbf{w} \leftarrow [\mathbf{1}^T, \mathbf{0}^T]^T$
3:    **while** $m < M$ **do**
4:        $m \leftarrow m+1$, $n \leftarrow 0$, $k \leftarrow 0$, $\boldsymbol{\alpha}_n = \boldsymbol{\gamma}_n = \mathbf{0}$,
5:        $\boldsymbol{\chi}_k = \boldsymbol{\psi}_k = \mathbf{0}$, $err_x \leftarrow 1/\epsilon$, $err_w \leftarrow 1/\epsilon$
6:        **while** $n < N_m$ and $err_x \geq T_{er}$ **do**
7:            $n \leftarrow n+1$, $\mathbf{x}_{old} \leftarrow \mathbf{x}_{\mathcal{S}^c}$
8:            Create: $\boldsymbol{\delta}_x \sim B(1, 1/2)$ with values $\pm 1$
9:            $\mathbf{x}_{\mathcal{S}^c}^{+} = \mathbf{x}_{\mathcal{S}^c} + \beta_m \boldsymbol{\delta}_x$, $\mathbf{x}_{\mathcal{S}^c}^{-} = \mathbf{x}_{\mathcal{S}^c} - \beta_m \boldsymbol{\delta}_x$
10:           $L_x^{+} = L\left(\mathbf{x}_{\mathcal{S}^c}^{+}, \mathbf{w}\right)$, $L_x^{-} = L\left(\mathbf{x}_{\mathcal{S}^c}^{-}, \mathbf{w}\right)$
11:           $\boldsymbol{\xi}_x = (L_x^{+} - L_x^{-})\mathbf{1} \oslash \boldsymbol{\delta}_x/(2\beta_m)$
12:           $\boldsymbol{\alpha}_n = b_1 \boldsymbol{\alpha}_{n-1} + (1-b_1)\boldsymbol{\xi}_x$,
13:           $\boldsymbol{\gamma}_n = b_2 \boldsymbol{\gamma}_{n-1} + (1-b_2)\boldsymbol{\xi}_x \odot \boldsymbol{\xi}_x$,
14:           $\mathbf{x}_{\mathcal{S}^c} = \mathbf{x}_{\mathcal{S}^c} - \tau \boldsymbol{\alpha}_n/(\sqrt{\boldsymbol{\gamma}_n} + \epsilon)$,
15:           $err_x = \|\mathbf{x}_{\mathcal{S}^c} - \mathbf{x}_{old}\|_2/(\|\mathbf{x}_{old}\|_2 + \epsilon)$
16:        **while** $k < N_m$ and $err_w \geq T_{er}$ **do**
17:            $k \leftarrow k+1$, $\mathbf{w}_{old} \leftarrow \mathbf{w}$
18:            Create: $\boldsymbol{\delta}_w \sim B(1, 1/2)$ with values $\pm 1$
19:            $\mathbf{w}^{+} = \mathbf{w} + \beta_m \boldsymbol{\delta}_w$, $\mathbf{w}^{-} = \mathbf{w} - \beta_m \boldsymbol{\delta}_w$
20:           $L_v^{+} = L\left(\mathbf{x}_{\mathcal{S}^c}, \mathbf{w}^{+}\right)$, $L_v^{-} = L\left(\mathbf{x}_{\mathcal{S}^c}, \mathbf{w}^{-}\right)$
21:           $\boldsymbol{\xi}_w = (L_v^{+} - L_v^{-})\mathbf{1} \oslash \boldsymbol{\delta}_w/(2\beta_m)$
22:           $\boldsymbol{\chi}_k = b_1 \boldsymbol{\chi}_{k-1} + (1-b_1)\boldsymbol{\xi}_w$,
23:           $\boldsymbol{\psi}_k = b_2 \boldsymbol{\psi}_{k-1} + (1-b_2)\boldsymbol{\xi}_w \odot \boldsymbol{\xi}_w$,
24:           $\mathbf{w} = \mathbf{w} - \tau \boldsymbol{\chi}_k/(\sqrt{\boldsymbol{\psi}_k} + \epsilon)$,
25:           $err_w = \|\mathbf{w} - \mathbf{w}_{old}\|_2/(\|\mathbf{w}_{old}\|_2 + \epsilon)$
26:        $Er(m) \leftarrow L(\mathbf{x}_{\mathcal{S}^c}, \mathbf{w})$
27:    **Output:** $\mathbf{Er}_{1:M}$, $\mathbf{x}_{\mathcal{S}^c}$, $\mathbf{w}$

---

After their initialization, we use an iterative process for the update of the loads $\mathbf{x}_{\mathcal{S}^c}$, while keeping the weights fixed. Randomness arises from the fact that the $\boldsymbol{\delta}$ vector is drawn from the Bernoulli distribution, $B(1,1/2)$, taking values $\pm 1$ (steps 8 & 18). For the update part (steps 12-14 & 22-24) Adam is used, whereas for the gradient approximation (since the cost function is not differential) we use a two-sided finite-difference method (FDM) [16], [17] (steps 9-11 & 19-21). Once the optimization of the loads is carried out, their values are fixed and the optimization of the weights is performed in a similar manner using Adam. For the latter algorithm, we used the original set of parameters proposed in [13] and only fine-tuned the initial learning rate $\tau$, as specified in Section IV (we did not use the bias-corrected first and second moment estimates-see [13] for more details). The process is repeated over $M$ values using a sequence $\boldsymbol{\beta} = [\beta_1, \ldots, \beta_M]$ with decreasing values. The latter process is known as smoothing. The symbols $\odot, \oslash$ denote element-wise multiplication and division, respectively, while the square root of a vector $\sqrt{\mathbf{x}}$

is also considered element-wise.

## IV. SIMULATION RESULTS

For the evaluation of the model we employ a 4A-24P element R-MAMP ($N_a = 4$ AEs and $N_p = 6$ PEs per AE) array and attempt to match the radiation pattern of a $4 \times 2$ URA (dipoles spaced at $\lambda/2$) at various azimuth and elevation angles. The center frequency is at 3 GHz, $R_a = 50\ \Omega$, whereas the spacing of the MAMP array's elements along the $y$-axis is $\lambda/5$. The parameters of the proposed AO-S3DBA are: $\beta_m = \beta_{m-1}/2$, $\beta_0 = 5$, $M = 13$; $\tau = 1.2$; $N_m = 1000$, $T_{er} = 10^{-4}$, $\epsilon = 10^{-8}$; $b_1 = 0.9$, $b_2 = 0.999$ (see [13]). In all figures, we have plotted the 3D beam patterns (normalized power), as well as the azimuth and elevation cut planes of both the URA and the MAMP array with the optimized loads-weights.

First, we evaluate the performance of AO-S3DBA at various rotation angles in the azimuth and elevation. In Fig. 1, we observe the successful rotation of the MAMP's beam at $(\phi, \theta) = (60°, 90°)$. Fig. 1 (a) demonstrates the 3D normalized power of the $4 \times 2$ URA and the R-MAMP. Furthermore, finer details on the controlled steering of the beam can be observed in the azimuth and elevation cut planes, which are shown in Fig. 1 (b) and 1 (c), respectively. Next, we attempt to reproduce the beam of the $4 \times 2$ URA, which is steered in both azimuth and elevation angles, 45° and 120°, respectively. Fig. 2 (a), demonstrates the resulting 3D normalized powers of the URA and the MAMP array, while in Fig. 2 (b) and 2 (c), we observe a very accurate matching at both azimuth and elevation cut planes. Moreover, in Fig. 3, we present results with no rotation of the beam, i.e., at direction $(\phi, \theta) = (90°, 90°)$. We should note that at this direction only (without rotation) the best approach is not to optimize the weights at all (we came to this conclusion after extensive simulations). Therefore, we omitted the second part of the Alg. 1, i.e., the optimization of its weights (steps 16-25) for this case only, and used the fixed initial weights instead. In Fig. 3 (a), we compare the 3D normalized powers of the MAMP array to the URA and in 3 (b), (c) we compare their azimuth and elevation cut planes. Finally, we calculate the total mismatch error as well as the error in the azimuth and elevation cut planes between the beam patterns. The error values are given in Tab. I. It is clear that the overall performance of the proposed algorithm is remarkable.

From all the experiments (and more that we performed but are not presented here due to space limitations), it is evident that: a) we can reproduce the performance of a URA beam with a R-MAMP array while saving 50% of AEs (compared to the URA), and b) the existence of the PEs produces a beam

TABLE I: Mismatch error (%) of the 4A-24P R-MAMP beam pattern emulating the beam of a $4 \times 2$ URA.
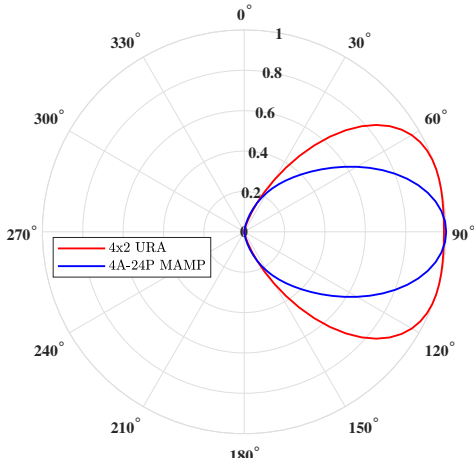
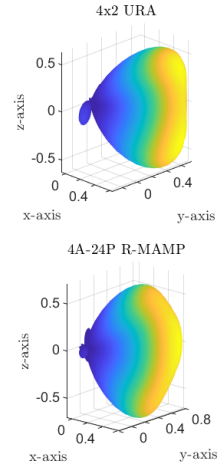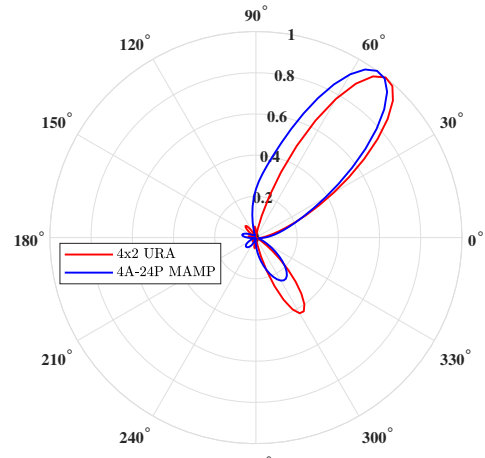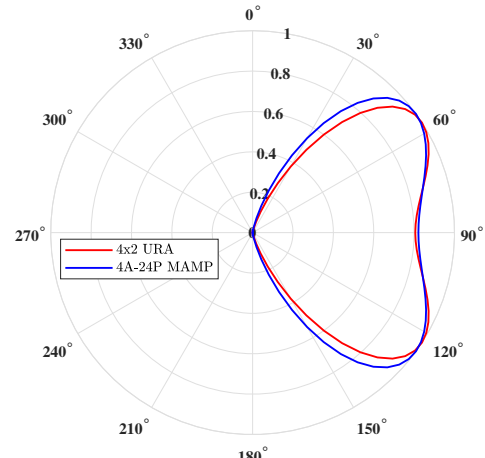| 3D direction | Total error | Azimuth error | Elevation error |
|---|---|---|---|
| $(60°, 90°)$ | 3.72 | 5.11 | 0.64 |
| $(45°, 120°)$ | 5.01 | 6.17 | 0.33 |
| $(90°, 90°)$ | 1.66 | 2.34 | 0.39 |
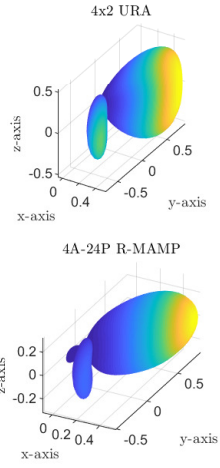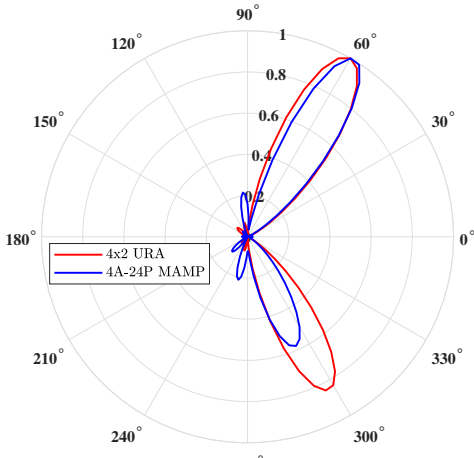
Fig. 1: Comparison of the: (a) 3D normalized powers, (b) azimuth cut plane and (c) elevation cut plane for a 4A-24P R-MAMP with optimized loads matched to a $4 \times 2$ URA at $(60°, 90°)$.



Fig. 2: Comparison of the: (a) 3D normalized power, (b) azimuth cut plane and (c) elevation cut plane for a 4A-24P R-MAMP with optimized loads matched to a $4 \times 2$ URA at $(45°, 120°)$.

that even outperforms that of the URA in some cases (reduced side-lobes or thinner beam).

## V. SUMMARY AND CONCLUSIONS

In this work, we demonstrated, for the first time, the 3D beamforming and steering of MAMP arrays. We proposed a stochastic optimization based algorithm, AO-S3DBA, which *controls the MAMP array's radiation pattern in both the azimuth and elevation directions* by alternating between the load and weight optimization. Moreover, we employed Adam, which is a popular stochastic accelerator, and managed to improve the convergence of AO-S3DBA without any compromise in the estimation accuracy. Simulated results show that we can successfully emulate the radiation pattern of a URA using a rectangular MAMP design with 50% less active elements, thus, reducing the cost and complexity of the array significantly.
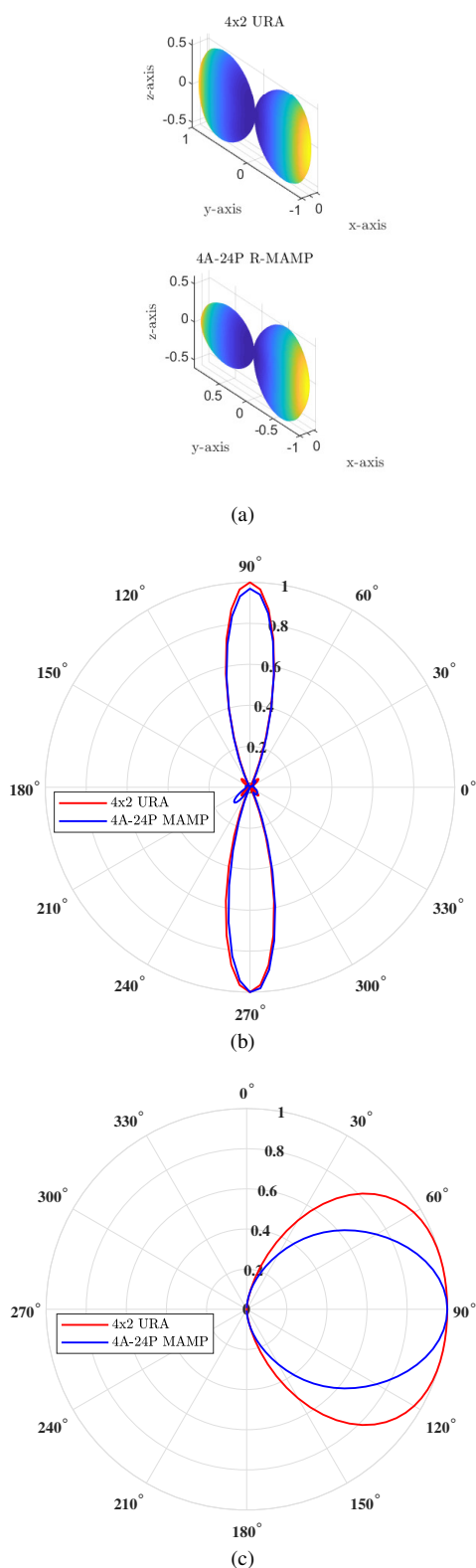


Fig. 3: Comparison of the: (a) 3D normalized power, (b) azimuth cut plane and (c) elevation cut plane for a 4A-24P R-MAMP with optimized loads matched to a $4 \times 2$ URA at $(90°, 90°)$.

## REFERENCES

[1] A. Kalis, A. G. Kanatas, and C. B. Papadias, *Parasitic Antenna Arrays for Wireless MIMO Systems*. Springer, 2014.

[2] K. Gyoda and T. Ohira, "Design of Electronically Steerable Passive Array Radiator (ESPAR) Antennas," in *IEEE Antennas and Propagation Society International Symposium*, vol. 2, July 2000, pp. 922–925.

[3] L. Zhou *et al.*, "Single-RF Multi-Antenna Transmission With Peak Power Constraint," *IEEE Transactions on Communications*, vol. 65, no. 12, pp. 5197–5208, Dec 2017.

[4] S. Uda, "On the Wireless Beam Of Short Electric Waves. (I)," *The Journal of the Institute of Electrical Engineers of Japan*, vol. 46, no. 452, pp. 273–282, 1926.

[5] S. Payami *et al.*, "Hybrid Beamforming With a Reduced Number of Phase Shifters for Massive MIMO Systems," *IEEE Transactions on Vehicular Technology*, vol. 67, no. 6, pp. 4843–4851, 2018.

[6] G. K. Papageorgiou *et al.*, "A Stochastic Optimization Approach to Hybrid Processing in Massive MIMO Systems," *IEEE Wireless Communications Letters*, pp. 1–1, 2020.

[7] G. K. Papageorgiou, D. Ntaikos, and C. B. Papadias, "Efficient Beamforming with Multi-Active Multi-Passive Antenna Arrays," in *2018 IEEE 19th International Workshop on Signal Processing Advances in Wireless Communications (SPAWC)*, June 2018, pp. 1–5.

[8] R. Qian, M. Sellathurai, and D. Wilcox, "A Study on MVDR Beamforming Applied to an ESPAR Antenna," *IEEE Signal Processing Letters*, vol. 22, no. 1, pp. 67–70, 2015.

[9] D. Wilcox *et al.*, "On Spatial Domain Cognitive Radio Using Single-radio Parasitic Antenna Arrays," *IEEE Journal on Selected Areas in Communications*, vol. 31, no. 3, pp. 571–580, 2013.

[10] H. L. Tian and D. Cheadle, "An Electronically Steerable Parasitic Array Radiator Antenna with Adaptive Beamforming Ability," in *2017 International Workshop on Electromagnetics: Applications and Student Innovation Competition*, July 2017, pp. 103–104.

[11] A. Kausar *et al.*, "Energy Efficient Switched Parasitic Array Antenna for 5G Networks and IoT," in *2016 Loughborough Antennas Propagation Conference (LAPC)*, Nov 2016, pp. 1–5.

[12] L. Marantis *et al.*, "A Printed Monopole ESPAR Antenna for Truck-to-Truck Communications," in *2017 International Workshop on Antenna Technology: Small Antennas, Innovative Structures, and Applications (iWAT)*, May 2017, pp. 239–242.

[13] D. P. Kingma and J. Ba, "Adam: A Method for Stochastic Optimization," *arXiv preprint arXiv:1412.6980*, 2014.

[14] C. A. Balanis, "Antenna Theory: A Review," *Proceedings of the IEEE*, vol. 80, no. 1, pp. 7–23, 1992.

[15] R. Vaughan and J. B. Andersen, *Channels, propagation and antennas for mobile communications*. Iet, 2003, vol. 50.

[16] J. C. Spall, *Introduction to Stochastic Search and Optimization: Estimation, Simulation, and Control*. John Wiley & Sons, 2005, vol. 65.

[17] P. Wilmott, S. Howison, and J. Dewynne, *The Mathematics of Financial Derivatives: a Student Introduction*. Cambridge University Press, 1995.